Chapter 6

Artificial Neural Network as a FPGA Trigger for a Detection of Neutrino-Induced Air Showers

Zbigniew Szadkowski, Dariusz Głas and
Krzysztof Pytel

Additional information is available at the end of the chapter

http://dx.doi.org/10.5772/63110

Abstract

Neutrinos play a fundamental role in the understanding of the origin of ultrahigh-energy cosmic rays (UHECR). They interact through charged and neutral currents in the atmosphere generating extensive air showers. However, the very low rate of events potentially generated by neutrinos is a significant challenge for detection techniques and requires both sophisticated algorithms and high-resolution hardware. We developed the FPGA trigger which is generated by a neural network. The algorithm can recognize various waveform types. It has been developed and tested on ADC traces of the Pierre Auger surface detectors. We developed the algorithm of artificial neural network on a MATLAB platform. Trained network that we implemented into the largest Cyclone V E FPGA was used for the prototype of the front-end board for the Auger-Prime. We tested several variants, and the Levenberg–Marquardt algorithm (trainlm) was the most efficient. The network was trained: (a) to recognize 'old' very inclined showers (real Auger data were used as patterns for both positive and negative markers: for reconstructed inclined showers and for triggered by time over threshold (ToT), respectively, (b) to recognize 'neutrino-induced showers'. Here, we used simulated data for positive markers and vertical real showers for negative ones.

Keywords: FPGA, trigger, cosmic rays, detection, neural network, neutrino, inclined showers, Pierre Auger Observatory

1. Introduction

The study of ultrahigh-energy cosmic rays (UHECR) of energy 10^{18}–10^{20} eV significantly speeds up both understanding and activities in both experimental as well as theoretical fields

of astroparticle physics [1]. Although many mysteries remain unsolved, such as the origin of the UHECRs, their production mechanism and composition, we are aware that it would be very difficult to explain the production of these energetic particles without associated fluxes of ultrahigh-energy neutrinos (UHEνs) [2, 3].

Generally, we can classify astrophysical models as: 'bottom-up' and 'top-down'. In the first one, protons and nuclei are accelerated from low to higher energies, while pions are produced in interactions of cosmic rays with matter or radiation at the source [4]. The 'top-down' models (based on Grand Unified Theories or Super-symmetries) consider that quark and gluon fragmentations of very heavy particles are a source of protons and neutrons, with an excess of pions compared with nucleons [5]. However, the Pierre Auger Observatory (**Figure 1**) rather disqualifies 'top-down' models because an observed photon stream is much lower than expected from the models [6]. From the other side, the Pierre Auger Observatory [7, 8] confirms the Greisen–Zatsepin–Kuzmin (GZK) cutoff [9, 10] observed also by Fly's Eye [11].

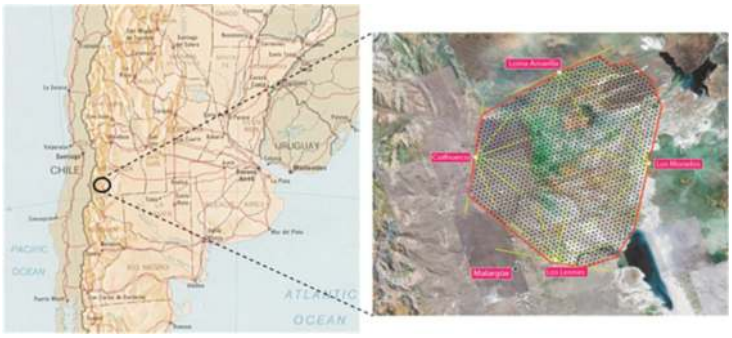

Figure 1. Location of the Southern part of the Pierre Auger Observatory.

In the downward-going channels, neutrinos of all flavours (generated via both charged and neutral current interactions) can develop extensive air showers in the entire path in the atmosphere, also very close to the ground [12].

In the Earth-skimming channel, showers can be induced by products of lepton decays after the interaction of an upward-going inside the Earth [13]. The surface detector of the Pierre Auger Observatory has potentially capabilities to detect neutrino-origin showers (for both the Earth-skimming and downward-going channels) from showers induced by regular cosmic rays for a large zenith angle ($\theta \geq 70°$) [14].

In the bottom-up scenarios, protons and nuclei are accelerated in astrophysical shocks, while pions are produced by cosmic ray interactions with matter or radiation at the source. In the top-down models, protons and neutrons are produced from quark and gluon fragmentations with a production of many more pions than nucleons.

The UHECR flux above ~5×10^{19} eV is significantly suppressed according to expectations based on the UHECRs interaction with the cosmic microwave background (CMB) radiation. For

http://dx.doi.org/10.5772/63110

primary protons, the photo-pion production is responsible for the GZK effect; thus, UHEvs are produced from decayed charged pions. However, their fluxes are doubtful and if the primaries are heavy nuclei, the UHEvs should be strongly suppressed [15].

Neutrinos can directly show sources of their production because there is no deflection in magnetic fields. Unlike photons, they travel inviolate from the sources and may give hints for production models. UHEvs can be detected with arrays of detectors at ground level that are currently being used to measure extensive showers produced by cosmic rays [16]. The main challenge is an extraction from the background, induced by regular cosmic rays showers initiated by neutrinos. Due to a very small neutrino cross section for interactions, a higher probability of a detection is at high zenith angles because a bigger atmosphere slant depth provides a thicker target for neutrino interactions. Inclined showers that begin their development deep in the atmosphere can be a signature of neutrino events.

2. Surface detector in the Pierre Auger Observatory

One of the most frequently used detection techniques is a ground array of water Cherenkov tanks, scintillator, calorimeters, utilizing water, liquid or solid plastics, lead as radiators, etc. The parameters of such a ground array (altitude, surface area, spacing between the detector stations) must be adapted to the energy range aimed for. The water Cherenkov tanks are filled by de-ionized water. Ultra-relativistic secondary from extensive air showers (EAS) passing through the water emits Cherenkov light. The light is converted by the PMTs into an electric signal for further processing. The tank is lined with the high-performance DuPont™ Tyvec® protective material (usually used as in a weather-resistant barrier) as a diffuse reflector on the walls. The reflector and high transparency of the super-pure water, with large attenuation length, assure multiple photon reflections and in consequence long electric signal as a response to the light excitation (**Figure 2**).

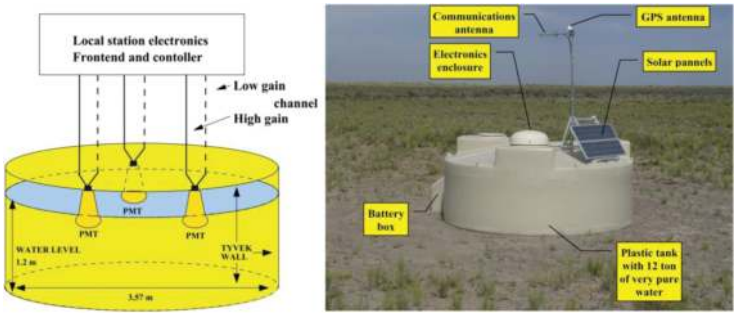

Figure 2. Water Cherenkov tank schematics. Each tank contains 12 tons of water as a radiator. The light is detected by three PMT, and each connected to a high- and a low-gain channel in the local station electronics.

EAS on the ground level hit usually several tanks. The number of hit tanks depends on the energy of the shower and the angle of arrival. The response of the surface detectors to EAS allows an estimation of the energy of the primary cosmic ray. This is obtained through the calculation of the integrated signal at the given distance from the shower axis. The distance is usually chosen to minimize shower-to-shower fluctuations (1000 m in the Pierre Auger Observatory). This signal, called hereafter S(1000) and expressed in vertical equivalent muon (VEM) units, is interpolated after a fit of a lateral distribution function to the observed signals in a given event. Simulations show that it does not depend much on the choice of the lateral distribution function. Calculation of the primary energy from S(1000) by simulation is an advanced topic and may depend on the modelling. The estimation of the primary energy from S(1000) by comparison with simulations is not a sufficient technique. The energy of showers is calculated from the SD data but calibrated from the FD data.

One of the crucial measured parameters allowing inferring characteristics of EAS is the timing of registered signals. 'Time shape' of a signal tells about the size of EAS and on a distance from the core, sharpness of rising edge enriches information on the muon composition, relative timing between neighbouring detectors determines the geometrical configuration and arrival direction of the shower. Time resolution should be good enough not to lose important time-dependent structure.

Muons tend to arrive earlier than electrons and photons and to create shower with relatively flat front, because they suffer much less scattering and so have more direct paths to the ground. Signal differences between muon and electron/photon components of EAS increases with the showers age. Inclined and deeply penetrating showers are muon rich. Muon flat front gives in PMTs a short, sharp response (electric spike). Electrons and photons give much smooth PMT signal profiles, which spread over longer interval. 'Rise time' measurements are the most robust diagnostics of composition for the surface array. Iron showers, which are both muon rich and develop higher in the atmosphere relative to proton showers, have a signal, arriving in a shorter time than that from a proton shower with the same total energy.

A practical realization of very high time resolution system meets significant difficulties. Digitalization of very wide range of signals with high speed requires not only expensive FADC but also very high-speed processing electronics. The measurement system should fetch a reasonable compromise between a speed and performance needed from the physics point of view and the costs, a level of complication, power consumption, longevity and reliability from the point of view of the practical implementation. The current technology provides a sampling of the analogue signals with the speed 40–100 Msps, with reasonable costs, high component integrity and expected reliability in long-term operation.

3. Triggers in the surface detector

The large background coming from small air showers, electronic noise and random coincidences imposes special constraints on triggers, which have to select EAS. Triggers have been accomplished in a hierarchical way both in hardware and in software to select possible

http://dx.doi.org/10.5772/63110

interesting events and verify their structure in the consecutive levels. A splitting of triggers on hardware and software implementation is a consequence of the compromise between the speed (the processing of high-rate signals possible by hardware only) and the performance of relatively complicated algorithms investigating timing and relationships between neighbouring detectors (a software realization, possible due to much lower event rate and not necessarily too complicated for a hardware implementation).

The cosmic ray particle flux generates ~2.5 kpps event rate in the water Cherenkov tank. PMT noise adds next few kpps rate. The total background rate (single muon + small showers + PMT dark noise) is estimated on the level ~5 kpps per station. The first level-trigger selects potentially interesting data from an uncorrelated background of several kpps to ~100 pps. The main tasks of the first-level trigger are clipping muon signals to reduce both: the trigger sensitivity to the primary composition and bias from small showers close to the detector, from which the signal is spread over relatively short time. The first function is motivated by the strong dependence of the muon content on the primary species, and the muon content of the shower providing the best handles of the primary composition. The second function is motivated by the increase in the time duration of the signal farther from the shower core. The first-level trigger reduces the contribution of muons to the trigger sum by truncating the pulse height at the programmable threshold and integrating the signal below the clip level. The integration of the truncated signal biases the trigger against nearby small showers, with energy deposit over short time interval. The parallel implementation accepts events with large energy deposition and neglecting their time structure, coming from close to the core of large showers.

The trigger/memory circuit registers and analyses the set of FADC samples in six channels corresponding to the profile of showers. The only high-gain sub-channel generates the trigger. The low-gain channel provides additional information, if the high-gain channel is saturated. The gain tuning of both sub-channels assures 15-bit dynamic range (each channel provides 10-bit dynamic range, with 5-bit overlapping).

Each surface detector generates two-level triggers (T1 and T2). T1 trigger works in two modes:

- a simple threshold trigger (TH) requiring threefold coincidences of three PMTs each above 1.75 I_{peak}^{VEM}. The TH rate is dynamically set on ~100 Hz by the adjustment of high voltages on PMTs. This trigger suppresses an atmospheric muons dependence. It is used to select large signals that are not necessarily spread in time.
- the 'time over threshold' (ToT), which needs at least 13 bins in 120 ADC-bins of a sliding window of 3 μs being above 0.2 I_{peak}^{VEM} threshold in coincidence in 2 out of 3 PMTs. This trigger is especially efficient for small signals spread in time, for example low-energy showers with a dominated EM component or for high-energy showers but far from the detector (**Figure 3**).

The T1 triggers start DAQ in each surface detector: event data are stored on a local memory for 10 s waiting for a possible T3 to be transferred to central data acquisition system (CDAS). T3 trigger is generated by CDAS, when there are spatial and temporal correlations between the local triggers.

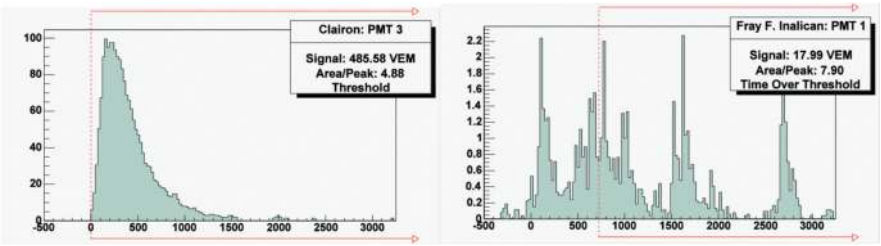

Figure 3. Sample of signals from the same event (#01307007). Signals from Clairon suggest that the shower core passed very close to this tank (Threshold trigger). Signals from Fray F. Inalican relatively weak and spread in time suggest far distance of this tank from the shower core time over threshold trigger).

4. Signal waveform analysis

In very inclined 'old' showers, the EM component is suppressed to a negligible level relatively early in a shower development. On a detection level, only the muon component survives as a muon 'pancake' of ~1 m thick. Such 'pancake' generates a very short signal in surface detectors with a very fast rising edge. These types of ADC traces (very fast jump from a pedestal level with an exponential attenuation tail) are relatively easy to recognize, especially by the algorithm based on the discrete cosine transform. The DCT trigger was already tested on the SD test detector in Malargüe (Argentina). The algorithm precisely can recognize signals of predefined shapes. The ANN algorithm is an alternative approach.

'Young' showers are spread in time over hundreds of nanoseconds. They contain also a part of EM component, which extends the signal waveforms in time. Nevertheless, the muonic component of 'young' showers overtakes the EM one and gives an early bump. The rising edge of the bump is softer than the 'old' showers, but this signal is also relatively quickly attenuated, till the EM component starts to give its own contribution. The ANN approach focuses on the early bump, to select traces potentially generated by neutrinos. Simulations of showers in CORSIKA and a calculation of the response of the surface detectors in offline showed that for neutrino showers (initiated either by ν_μ or ν_τ) for relatively big zenith angle (i.e. >70°) and low altitude (<9 km) give relatively short signal waveforms and they can be analysed also by 16-point pattern engines.

5. CORSIKA and offline simulations

5.1. Artificial neuron network: data preparation

The main motivation of an ANN implementation as a shower trigger is that up to now, and the entire array did not register any neutrino-induced event. Our idea was to use the ANN approach as a pattern recognition technique. The input data for the ANN are simulated traces

http://dx.doi.org/10.5772/63110

of protons and muon neutrinos, which hit the atmosphere at high zenith angles—80°, 85° and 89°, respectively. The chosen energies of primary particles are 3×10^8, 10^9, 3×10^9 and 10^{10} GeV, respectively. The distances from the place of the first interaction to the detector used for simulations are dependent of the angle and the type of particle (**Table 1**). We decided not to simulate protons that are very close to the detector, because the probability that the protons will not interact to detector is very low. Additionally, traces produced by this kind of interactions may also include the electromagnetic part of the shower. These traces would look completely different than the rest and may significantly decrease the efficiency of the ANN.

		500	1000	2000	3000	4000	5000	10,000
80°	p			YES	YES	YES		
	ν	YES	YES	YES	YES	YES		
85°	p			YES	YES	YES	YES	
	ν	YES	YES	YES	YES	YES	YES	
89°	p			YES	YES	YES	YES	YES
	ν	YES	YES	YES	YES	YES	YES	YES

All distances are in g/cm^2. Distances are correlated with an angle.

Table 1. Distances from the place of the first interaction to detector for proton and muon neutrinos in dependence of zenith angle.

We investigated 120 different categories of events (30 active categories from **Table 1** × 4 energies). These categories are used as input by the CORSIKA simulation platform. The CORSIKA program simulates the cosmic ray shower initiated by the specific particle. The result of this simulation is the distribution of the position and energies of the particles on the level of the detector. Simulations are relatively fast. The simulated cosmic ray showers are the input for the offline package, which provides a response to the water Cherenkov detector and generates the ADC traces (signal waveforms). These simulations are very time-consuming. As a result, we obtained simulated traces from the photo-multipliers, as if they were triggered by a standard T1 trigger. We have proven that a 16-point input is sufficient for the ANN pattern recognition [17] (**Figure 4**). The next step was to find in the 16-point trace, which corresponds

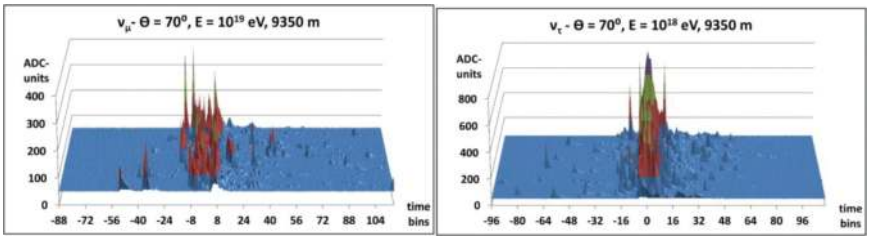

Figure 4. Simulated signal waveforms for 10^{19} and 10^{18} eV for initial ν_μ and ν_τ, respectively, at 9350 m and 70° zenith angle.

to triggered events. To see the beginning of the event clearly, we decided that first two points should be on the pedestal level. Afterwards, we subtracted the pedestal level from all used data.

5.2. Training and testing steps

For a training procedure, we decided to use half of the data available for the testing procedure. We arranged the data, to have proton and neutrino traces alternately. The proton traces were treated as negative signals ('0' for the ANN), and the neutrino traces were treated as positive ones ('1' for the ANN). This step allowed the ANN to be taught faster and to have fewer errors while training. The testing procedure consisted of assigning a specific value to the trace. This value depends on the coefficients of the trained ANN. If the value is greater than the threshold, the trace is treated as a neutrino trace; otherwise, it is treated as a proton trace. The efficiency of the neutrino recognition with a specific threshold level can be defined as the number of neutrino traces recognized correctly divided by the number of all neutrino traces. The proton mistakes level is defined as the number of proton traces treated as neutrino traces divided by the number of all proton traces.

The testing procedure was divided into two stages. First, we wanted to find out if we could use the data from the specific category to distinguish muon neutrinos and protons for all the angles or all the energies. Simulated data contains only three different angles: 80°, 85° and 89°, respectively, but we did not expect the zenith angle of the particle to be exactly like them. If the ANN trained on the specific category with an angle of 85° can also distinguish neutrinos and protons for 89° and 80° with acceptable efficiency, we assumed it could also distinguish protons and neutrinos for a full angle range: 80°–89°. The same assumptions have been established for energies. The ANN had been also trained by the data of the specific energy, and it was then tested on the other values of the chosen parameter. The second step of the testing procedure consisted of training the ANN by the randomly taken data from all categories.

5.3. Increasing the efficiency

The efficiency of the ANN strongly depends on the data used for training. The positive and negative signals should be as different as possible in order to increase the distinction of proton and neutrino traces. Our first results have shown that ANN does not work properly. There was no separation between protons and neutrinos. When we looked at the data we used for teaching the ANN, we found that some of the neutrino and proton traces looked very similar to each other. Moreover, the simulated traces produced by neutrino showers with various distances to the detector, but with the same energy and angle, and were diametrically different. We observed the same effect in the other angles and energies (**Figure 5**) and in the traces produced by protons. This effect is directly connected to the electromagnetic (EM) part of the shower. If the distance to the detector is short, the EM part of the shower gives a second component in the traces, in addition to the standard muonic one.

http://dx.doi.org/10.5772/63110

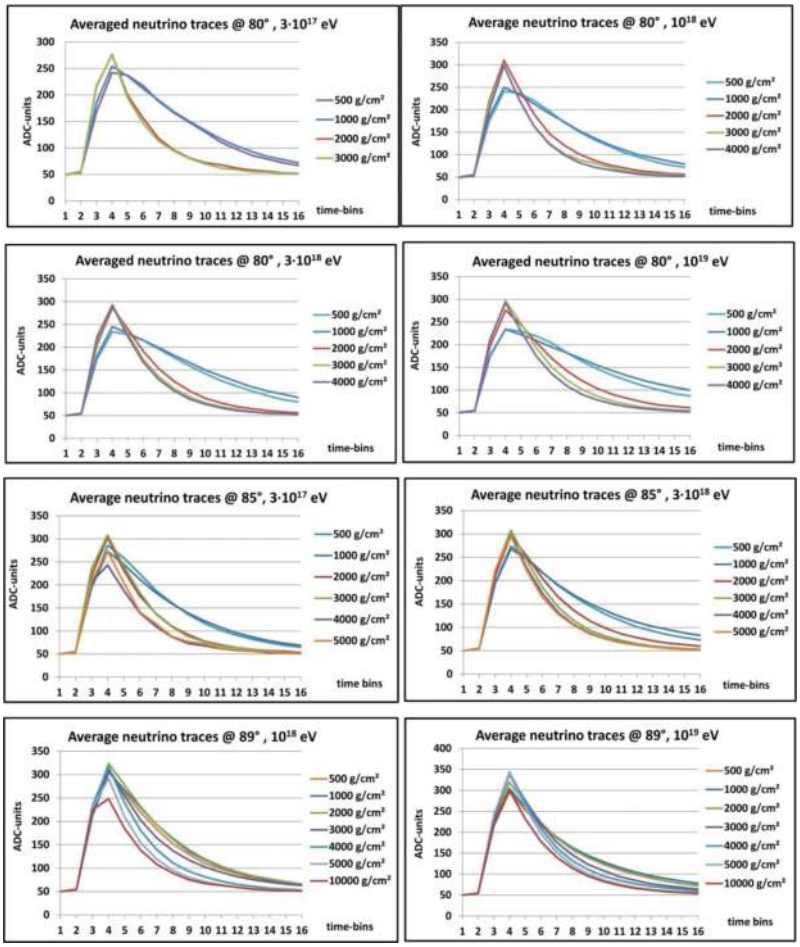

Figure 5. Plots contain averaged muon neutrino signal waveforms (ADC traces) for various angles, energies and initialization points. The exponents of the traces at distances 500 and 1000 g/cm^2 are different than on the rest of distances. This effect does not depend on the energy and slightly depend on the angle.

At high zenith angles, the proton showers should not have the EM component, because it should disappear after 2000–3000 g/cm^2. Old neutrino showers looked like old proton–neutrino showers, so we decided to separate the data and focus on recognizing only the young neutrino showers, where the EM component was still visible. We also decided to remove proton showers with a visible EM component, because the traces that they generated looked similar to traces generated by young neutrino showers.

Moreover, for these showers, the probability of occurrence at this angle was low. The data we decided to keep were for all neutrino traces with distances 500 and 1000 g/cm^2, and all proton traces with two maximal distances for each angle.

Figure 6 shows the average traces for data at 80 after the separation. Neutrino and proton traces have completely different shapes, so it should be easier to recognize the neutrino traces when ANN is learned and tested based on this data.

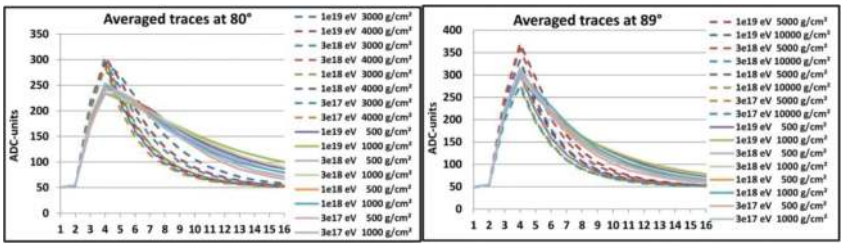

Figure 6. Plots show the differences between the traces produced by old proton showers (without markers) and young neutrino showers (with markers). Traces can be recognized on a base of exponential attenuation factors especially for relatively low angles (80°). Graphs show that for large zenith angles and very wide energy ranges, 'old' proton showers are attenuated faster than 'young' neutrino showers.

Figure 7 shows the histogram of the average exponents of rejected and accepted proton and neutrino categories. We can see that the exponents of the rejected neutrino categories correspond with exponents of the accepted proton categories. This was probably the main reason for the low distinction of protons and neutrinos by ANN. Additionally, the average exponents of the accepted proton and neutrino categories are separated.

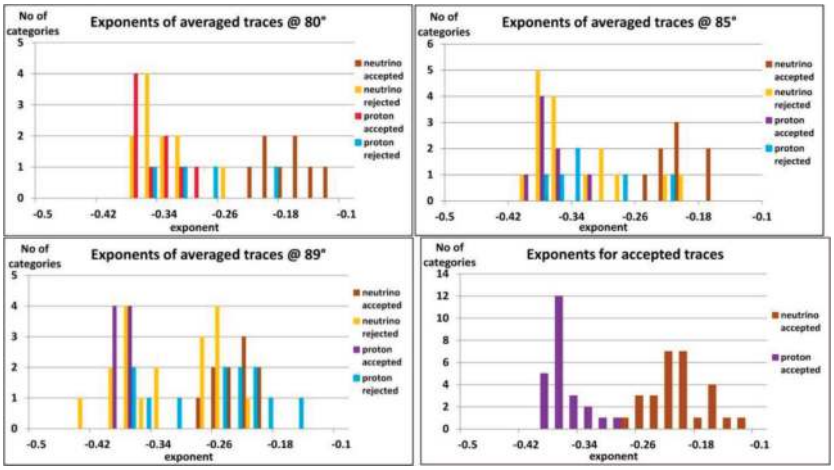

Figure 7. Histograms of exponents of rejected and accepted traces for protons and neutrinos. The accepted neutrino traces exponents are separated from the accepted proton traces exponents.

The rejected neutrino traces look very similar to traces made by old proton showers. This may cause problems with ANN training and may increase the level of the proton traces recognized

http://dx.doi.org/10.5772/63110

as neutrino traces by the ANN. Nevertheless, the last graph shows that a proton–neutrino pattern recognition seems to be possible. Training by patterns for only 'old' proton showers and 'young' neutrino showers seems to be justified as protons start their interactions just in the beginning of the atmosphere, while the probability of neutrino interactions high in the atmosphere is negligible.

6. MATLAB analysis

Figure 8 shows the ANN efficiency versus angles and energies. If all data from simulation, independently of the origin point (of old and young, and of both proton and neutrino events), are taken for teaching, the network recognitions is poor. Proton background (spuriously recognized) is relatively high, and the efficiency of the neutrino event recognition is also poor. However, if in the teaching process we use dedicated young neutrino and old proton patterns the recognition efficiency significantly increases. The ANN tested on non-separated traces has problems distinguishing the proton and neutrinos on every level of the threshold. The efficiency of a recognition of neutrino traces and the level of proton mistakes differ only slightly. The ANN, tested on the separated traces, can recognize protons and neutrinos with acceptable efficiency. The proton mistakes level is much lower than the recognition efficiency of neutrino traces; moreover, the efficiency of finding neutrino traces is higher than in the previous case.

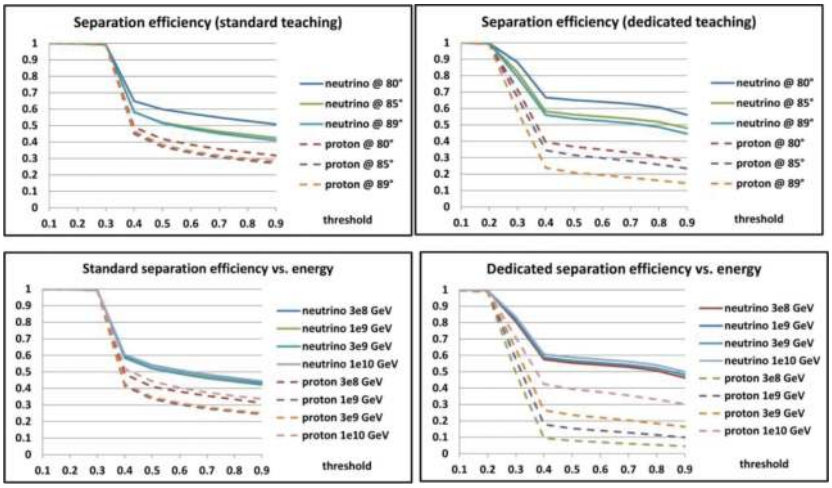

Figure 8. The graphs show the separation efficiency of the neutrino events from the proton background as a function of the threshold for various angles and energies of the initial particle. The 'standard' graphs show the efficiency for a network teaching on the basis of a wide range of initial points of the first interaction. The 'dedicated' graphs show the efficiency when the network is trained by patterns corresponding to 'young' neutrino events and 'old' proton ones. A higher level of the proton background (spuriously recognized) for lower angles (80°) comes with a higher probability of the EM.

Right graph on **Figure 8** shows our choice for future tests. The efficiency of neutrino recognition is independent of energy and on a relatively high level (0.5–0.6), while proton spuriously recognized events are on a low level especially for low energies: 3×10^8–10^9 GeV. For higher energies, signals are generally stronger, and there is a much higher probability of their recognition by a standard threshold triggers.

Preliminary results show that more complicated networks do not improve a pattern recognition on a level that justified an increment of structure complication, resources occupancy, or, finally, of much greater requirements for a budget. We did not notice that the structure from **Figure 9a** was superior over **Figure 9b**. Moreover, the much more complicated networks, 24-16-1 and 36-24-1 showed minimal improvement in comparison with a much simpler network, 12-8-1. The networks 24-16-1, and especially 36-24-1, require a huge amount of FPGA resources (especially DSP blocks). The biggest chip 5CEA9F31I7 from the low-cost FPGA family Cyclone® V contains 684 of 18 × 18 DSP embedded multipliers, while the biggest chip 5AGXB7 from the Arria® V family contains 2312 of 18 × 18 DSP blocks (the biggest chip 10AT115 from the Arria® 10 medium-cost FPGA family contains 3036 of 18 × 19 multipliers). However, the prices of Arria FPGAs are unacceptable for a mass production of the front-end boards (**Figure 12**).

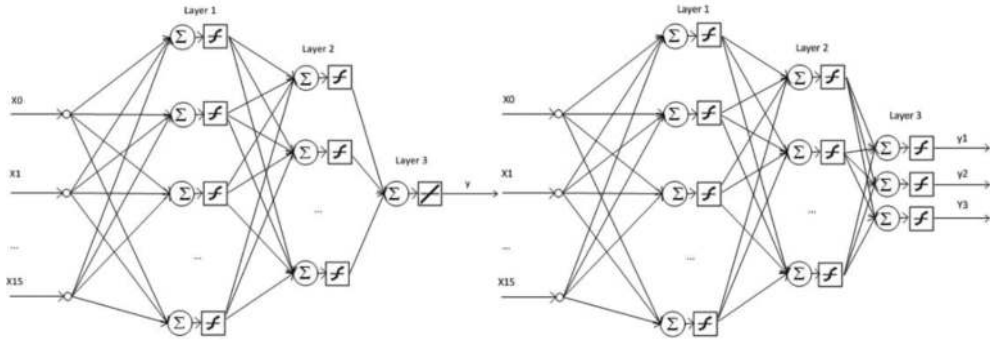

Figure 9. An internal structure of an FPGA neuron network with tansig function scaling output neuron data between consecutive layers. This right net contains more advanced last layer, which tries to separate patterns with higher efficiency.

Independently of the FPGA prices, the crucial factor becomes power consumption. Mid-size FPGAs (Arria® V or 10 as well as Stratix® IV or V families) are optimized for maximum performance, while a power budget is not a priority. Nevertheless, our estimations show that more complicated networks 24-16-1 or 36-24-1 minimally improve a neutrino–proton separation; a significantly higher cost for the implementation these networks with a much more expensive FPGA is not justified (**Figure 11**).

For training of the neural networks, we used real Auger ADC traces triggered either by the TH-T1 or by the ToT trigger [14] (**Figure 10**). Due to relatively high thresholds, the TH-T1

http://dx.doi.org/10.5772/63110

trigger trespasses relatively strong signals. We know that up to now the Pierre Auger Observatory did not register any event potentially generated by neutrinos. The reason may be the configuration of the standard trigger (threefold coincidence in a single time slot), which does not take into account a de-synchronization of signals [18]. The probability of de-synchronization increases for higher sampling frequencies. The Cherenkov light can simultaneously reach all PMT only for specific conditions of the angle and the input position of the trespassing ultra-relativistic particle due to a geometry of the surface detector (<8%).

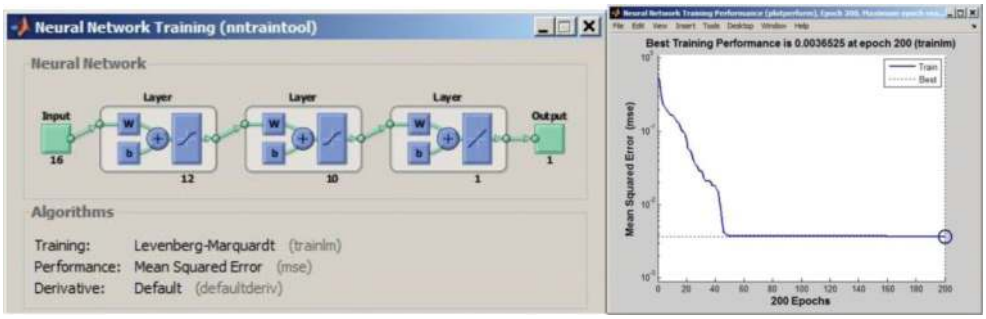

Figure 10. The MATLAB neural network tool used for teaching according to Levenberg-Marquardt algorithm (left). The right graph shows a convergence during training.

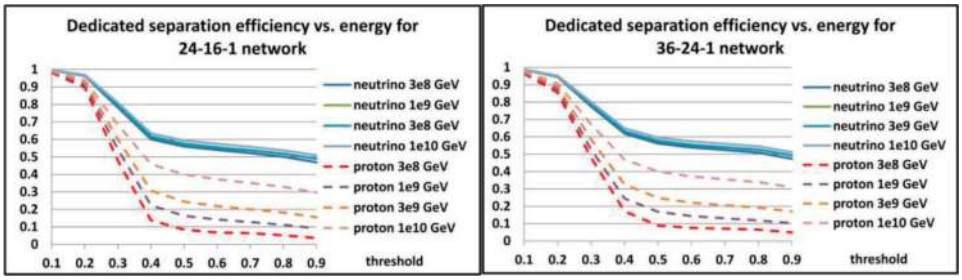

Figure 11. Efficiency of neutrino-proton separation for 24-16-1 and 36-24-1 neural networks.

Practically only twofold coincidences can give events of very inclined showers. A reflected light reaches the third PMT with a delay 'firing' the PMT in later time slots and also too low amplitude of signals for low energetic initial particles maybe the reason. We were teaching the network to recognize patterns with decreased amplitudes. The database was artificially extended by the real signal waveforms with reduced amplitudes by factors of 0.67, 0.5 and 0.25, respectively, keeping the same pedestals and shapes.

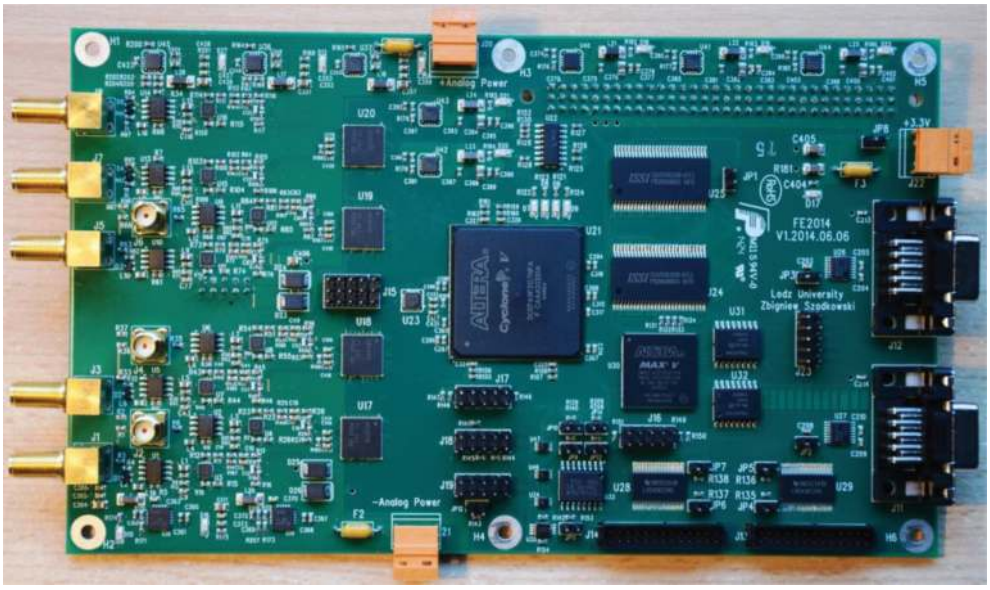

Figure 12. The front-end board with Cyclone V E FPGA used for high-resolution tests in the Pierre Auger Engineering Array.

7. FPGA implementation

Figure 9 shows an internal structure of an FPGA neuron network with tansig function scaling output neuron data between consecutive layers. Each neuron (**Figure 13**) output (before a connection to the next layer) has to be scaled by a neural transfer function to focus a response on a most important data region. Typically, the transfer function is a hyperbolic tangent sigmoid (tansig—**Figure 14**). The constant coefficients were implemented in the ROM (**Figure 17**). We selected dual-port memory (two addresses inputs and two independent data outputs by the same content) to reduce a resource occupancy.

The fundamental algorithm for each neuron is as follows:

$$Neuron_{out} = \sum_{k=0}^{n-1} ADC_k \times C_{k,layer} + bias_{k,layer} \tag{1}$$

We implemented 16,384-word dual-port ROM with 14-bit output in order to keep a sufficient accuracy with a reasonable size of the embedded memory

http://dx.doi.org/10.5772/63110

$$f_{index} = \frac{2}{1 + e^{-2\frac{index-8192}{sf}}} - 1 \tag{2}$$

The ADC output is connected to 12-bit shift registers whose sequential outputs drive neuron inputs. A teaching process of MATLAB generates a set of coefficients represented by 'double' variables. An implementation of floating point coefficients in the FPGA slows down significantly a register performance and dramatically increases resource occupancy. Practically, the accuracy in a fixed-point approach is absolutely sufficient. There is no need to calculate an individual neuron response in a very high precision due to general uncertainties in this estimation process.

At least two embedded DSP multipliers have to be used for a single multiplication of 12-bit input data. If we select 32-bit data width, the maximal width of the coefficients is 20-bit.

Figure 14 shows shapes of tansig function for various parameterizations. For our training data, the best scaling factor is sf = 1536, which corresponds to the range of (−5.33,…,+5.33).

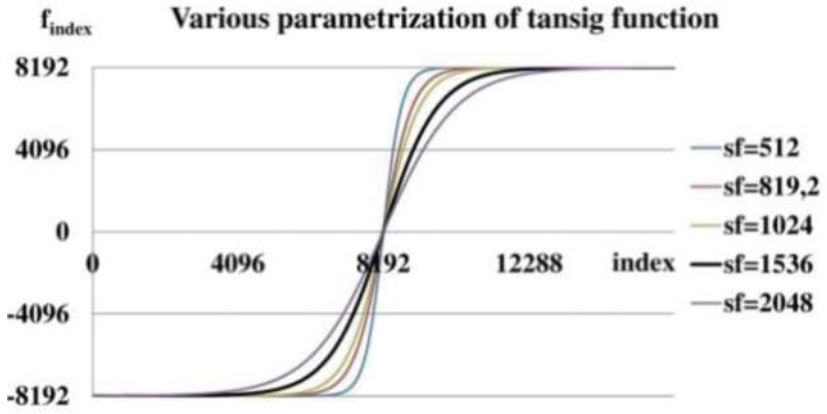

Figure 13. Altera IP floating-point procedures. A multiplication of 64-bit variables requires at least five clock cycles, a summation at least seven clock cycles, respectively.

A floating-point variables in the FPGA contain from sign bit (MSB), mantisa and exponent. Double variables require 64-bit representations (52-bit mantisa and 11-bit exponent). Summation and multiplication require at least seven and five clock cycles latency, respectively (**Figure 13**).

Signed variables in the FPGA logic require two-component representation. Altera provides fixed-point IP-core routine (ALTMULT_ADD) for four parallel multiplications and partial results summation (**Figure 15**). In order to keep 32-bit output size, coefficients must be 18-bit only (**Figure 16**).

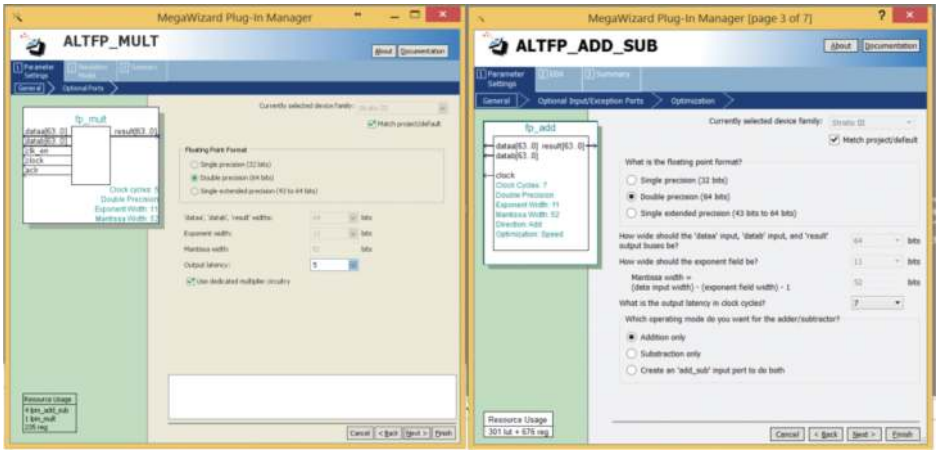

Figure 14. Tested parameterizations of tansig function for the best optimization.

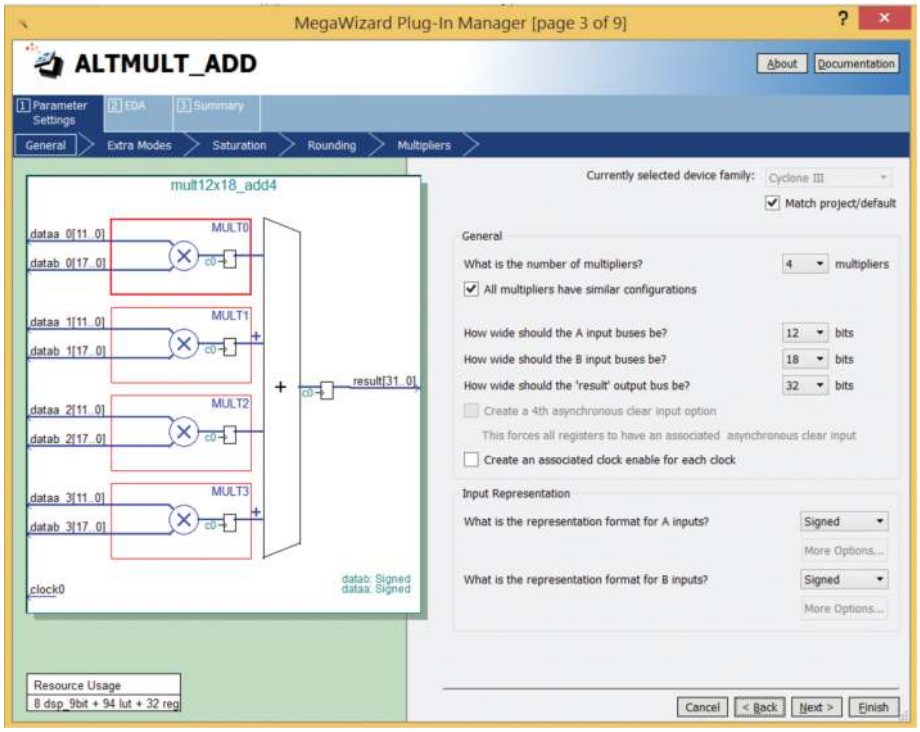

Figure 15. Altera ALTMULT_ADD IP-core procedure for a neural implementation.

http://dx.doi.org/10.5772/63110

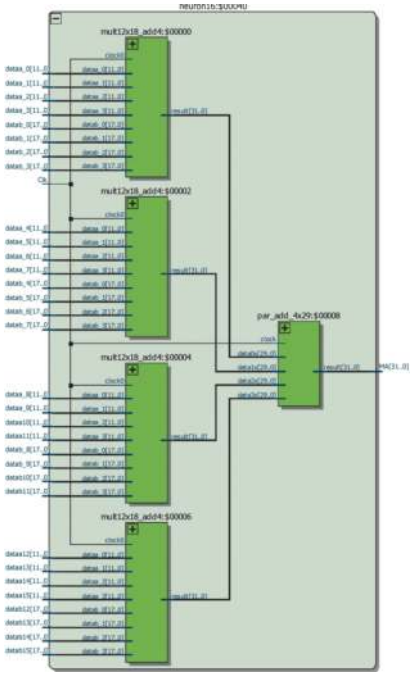

Figure 16. An internal structure of the 16-point FPGA neuron.

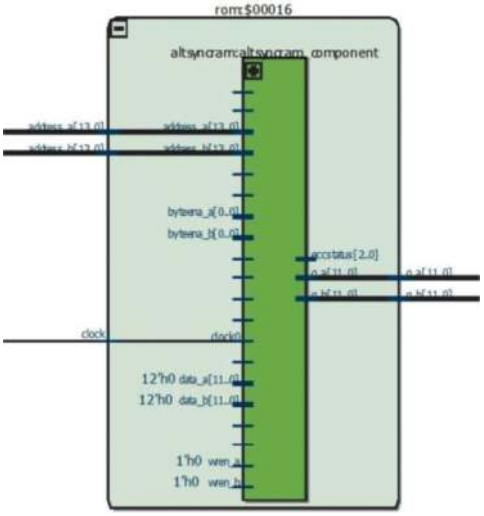

Figure 17. An implementation of the tansig function into ROM (above).

Layer	SFS	SFL	SFX	SFB	SHP	SHN
1	2	131,072	8	524,288	–	6
2	4	32,768	8	32,768	14	1
3	2	32,768	2	32,768	13	1

Table 2. Scaling, suppression and shift factors.

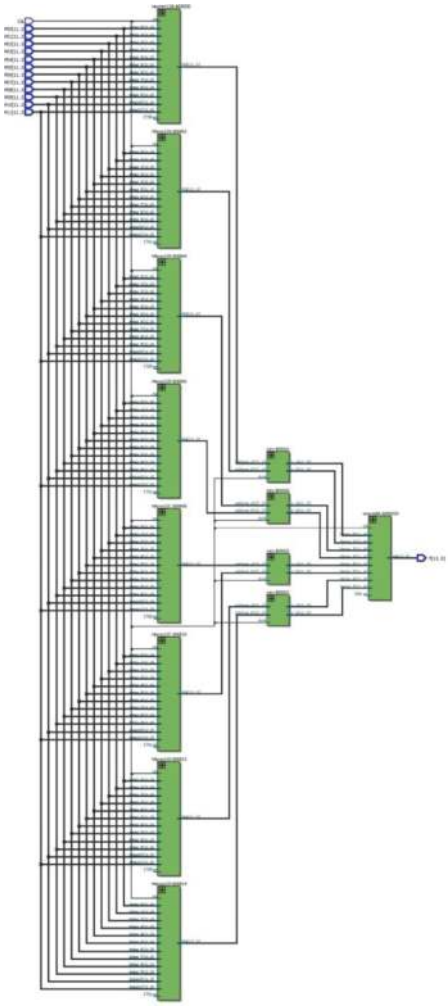

Figure 18. A structure of connections in two last layers: eight 12-input neurons + 4 ROM blocks with tansig functions + the last 8-input neuron (left graph).

Table 2 shows all factors for scaling, suppressions and finally shifts of data. At first, coefficients (coeff and bias) calculated by MATLAB are suppressed [by the factors SFS and SFX, respectively, to get a range (−1.0,…+1.0)]. Next, they are scaled by factors SFL and SFB, respectively.

$$coeff_{k,layer,fixed-point} = coeff_{k,layer}\frac{SFL}{SFS} \tag{3}$$

$$bias_{k,layer,fixed-point} = bias_{k,layer}\frac{SFB}{SFX} \tag{4}$$

The 32-bit signed output of neuron (starting from the second layer) is shifted right before a summation with the bias due to very large values from the tansig transfer function (mostly either ~−8192 or ~8191).

$$P = \left(\sum_{k=0}^{n-1} ADC_k \times C_{k,layer}\right) \rangle\rangle SHP\,address_{k,layer} = \left(P\rangle\rangle SHP\right) + 8192 \tag{5}$$

Addresses for tansig function are additionally optimized to use the most sensitive function response region. The highest bits from the neuron are neglected as irrelevant for a big argument of the tansig transfer function. Addresses are cropped to the range 0,…,16,383 (**Figure 18**).

8. Simulations for the FPGA

A relatively old tool—the Quartus simulator was used for simulations as much faster than currently recommended ModelSim. The structure of the neuron network has been implemented into several FPGA families: Cyclone III, Stratix III and Cyclone V. A response of neural network on trained patterns was verified for 16-point inputs with fixed coefficients calculated in MATLAB.

Figure 19 show Quartus simulations of selected traces. Inclined showers correspond to positive markers, and vertical showers correspond to negative markers. A recognition of selected patterns is on very high level. We simulated 160 events (totally 122,880 samples). One hundred and sixty one patterns were recognized as positive markers: 160 inclined showers and only a single false event. Among 160 vertical showers used as reference ones (with negative markers), the network recognized 39 events faulty; however, 12 with high amplitudes, which should be detected also by a standard trigger.

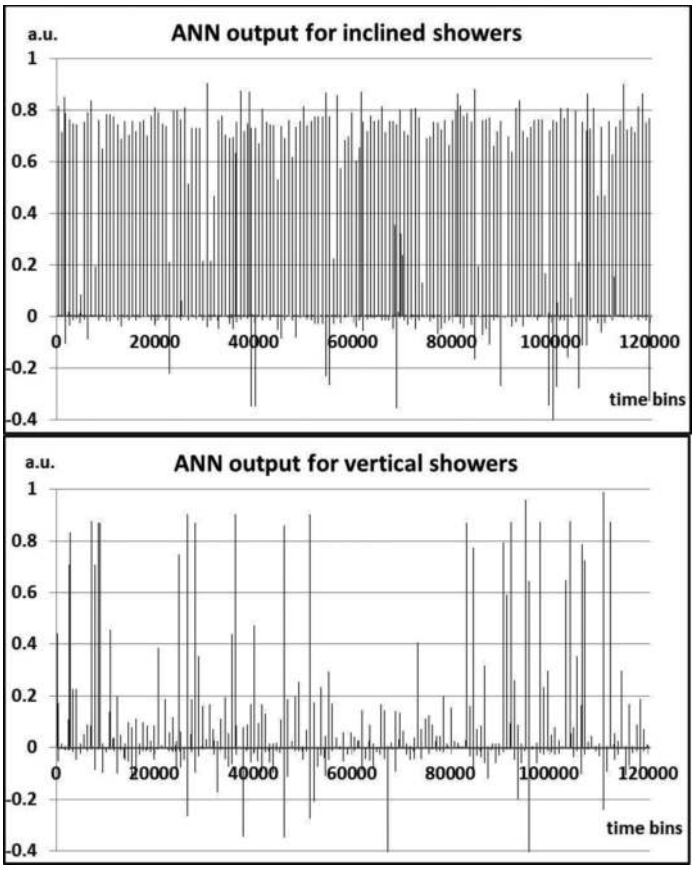

Figure 19. Graphs show the output of 12-8-1 neural network for positive-marked inclined showers (upper graph) and negative-marked vertical showers. Each graph shows 122,880 samples (768 samples/event). Outputs from the third neural layer are scaled to a range (−1,…,+1).

9. Conclusion

We simulated several showers initialized by ν_μ and ν_τ using the CORSIKA package. Output CORSIKA data (particles energies, momentum, coordinates, etc.) calculated for 1450 m a.s.l (a level of the Pierre Auger Observatory) were used offline package for simulations of a surface detector response, that is shape of ADC traces after a digitization of PMTs Cherenkov light-induced signals. These ADC waveforms were the patterns for a training process of the neural network. Analysis of results for Cyclone V E FPGA 5CEFA7F31I7 is very promising. It shows that the ANN algorithm can recognize neutrino events that are at present neglected by the standard Auger triggers.

http://dx.doi.org/10.5772/63110

The recognition efficiency of the neutrino traces by the ANN algorithm strongly depends on the differences between the data used for the ANN training. If we teach the ANN with the data containing only traces produced by young neutrino and old proton cosmic air showers, we can reach an acceptable level of recognition. Moreover, we can distinguish protons and neutrinos, which means that the ANN works on a very promising level.

Acknowledgements

This work is supported by the National Science Centre (Poland) under NCN Grant No. 2013/08/M/ST9/00322. The authors would like to thank the Pierre Auger Collaboration for an opportunity of using the CORSIKA and offline simulation packages.

Author details

Zbigniew Szadkowski*, Dariusz Głas and Krzysztof Pytel

*Address all correspondence to: zszadkow@kfd2.phys.uni.lodz.pl

Department of Physics and Applied Informatics, University of Łódź, Łódź, Poland

References

[1] M. Nagano, A. Watson. Observations and implications of the ultrahigh-energy cosmic rays. Rev. Mod. Phys. 2000;72(3):689–732. doi:10.1103/RevModPhys.72.689

[2] V. S. Berezinsky, A. Y. Smirnov. Cosmic neutrinos of ultrahigh energies and detection possibility. Astrophys. Space Sci. 1975;32(2):461482. doi:10.1007/BF00643157[2]

[3] F. Halzen, D. Hooper. High-energy neutrino astronomy: the cosmic ray connection. Rep. Progr. Phys. 2002;65(7):1025. doi:10.1088/0034-4885/65/7/201

[4] J. K. Becker. High-energy neutrinos in the context of multi-messenger astrophysics. Phys. Rep. 2008;458(4–5):173246. doi:10.1016/j.physrep.2007.10.006

[5] P. Bhattacharjee, G. Sigl. Origin and propagation of extremely high-energy cosmic rays. Phys. Rep. 2000;327(3–4):109–247. doi:10.1016/S0370-1573(99)00101-5

[6] J. Abraham et al. [Pierre Auger Collaboration]. Upper limit on the cosmic-ray photon fraction at EeV energies from the Pierre Auger Observatory. Astropart. Phys. 2009;31:399–406. doi:10.1016/j.astropartphys.2009.04.003

[7] J. Abraham et al. [Pierre Auger Collaboration]. Properties and performance of the prototype instrument for the Pierre Auger Observatory. Nucl. Instrum. Methods. 2004;A523(1–2):5095. doi:10.1016/j.nima.2003.12.012

[8] J. Abraham et al. [Pierre Auger Collaboration]. Observation of the suppression of the flux of cosmic rays above 4×10^{19} eV. Phys. Rev. Lett. 2008;101(6):061101. doi:10.1103/PhysRevLett.101.061101

[9] K. Greisen. End to the cosmic-ray spectrum. Phys. Rev. Lett. 1966;16:748–750. [9] doi: 10.1103/PhysRevLett.16.748

[10] G. T. Zatsepin, V. A. Kuzmin. Upper limit of the spectrum of cosmic rays. Pisma v Zhurnal Eksperimentalnoi i Teoreticheskoi Fiziki. 1966;4:114. WOS:A19668298400011

[11] R. U. Abbasi et al. [Hi-Res Fly's Eye Collaboration]. First observation of the Greisen–Zatsepin–Kuzmin suppression. Phys. Rev. Lett. 2008;100(10):101101. [11] doi:10.1103/PhysRevLett.100.101101

[12] K. S. Capelle, J. W. Cronin, G. Parente, E. Zas. On the detection of ultra high energy neutrinos with the Auger Observatory. Astropart. Phys. 1998;8(4):321328. [12] doi: 10.1016/S0927-6505(97)00059-5

[13] X. Bertou, P. Billoir, O. Deligny, C. Lachaud, A. Letessier-Selvon. Tau neutrinos in the auger observatory: a new window to UHECR sources. Astropart. Phys. 2002;17(2): 183193. doi:10.1016/S0927-6505(01)00147-5

[14] J. Abraham et al. [Pierre Auger Collaboration]. Trigger and aperture of the surface detector array of the Pierre Auger Observatory. Nucl. Instrum. Methods. 2010;A613:29–39. doi:10.1016/j.nima.2009.11.018

[15] K. Kotera, D. Allard, A. V. Olinto. Cosmogenic neutrinos: parameter space and detectability from PeV to ZeV. JCAP. 2010;20(10):013. doi: 10.1088/1475-7516/2010/10/013

[16] E. Zas. Neutrino detection with inclined air showers. New J. Phys. 2005;7:130. doi: 10.1088/1367-2630/7/1/130

[17] Z. Szadkowski, K. Pytel. Artificial neural network as a FPGA trigger for a detection of very inclined air showers. IEEE Trans. Nucl. Sci. 2015;62(3):1002–1009. doi:10.1109/TNS.2015.2421412

[18] Z. Szadkowski. Optimization of the detection of very inclined showers using a spectral DCT trigger in arrays of surface detectors. IEEE Trans. Nucl. Sci. 2013;60(5):3647–3653. doi:10.1109/TNS.2013.2280639